Journal of Energy Storage 84 (2024) 110995

Contents lists available at ScienceDirect

Journal of Energy Storage

journal homepage: www.elsevier.com/locate/est

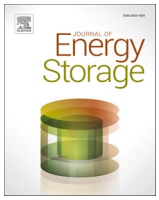

Research papers

Development of novel form-stable PCM-biochar composites and detailed characterization of their morphological, chemical and thermal properties

Dudul Das [a], Ondrej Masek [b], Manosh C. Paul [a,*]

[a] Systems, Power & Energy Research Division, James Watt School of Engineering, University of Glasgow, UK
[b] UK Biochar Research Centre, School of Geosciences, University of Edinburgh, Edinburgh, UK

ARTICLE INFO

Keywords:
Phase change material
Form-stable composite
Thermal energy storage
Thermo-chemical characterization
Enthalpy of phase transition
Photothermal conversion

ABSTRACT

Storing heat with phase change materials has the potential for several modern-day applications such as building thermal regulation, isothermal solar drying, electronic cooling, etc. However, to suitably incorporate latent heat energy storage systems, the challenges of leakage and low thermal conductivity of these materials need to be addressed. In this direction, biochar derived from abundantly available biomass feedstocks has been explored to develop form-stable, environmentally compatible energy storage materials. Biochar has been derived from wheat straw and softwood and has been analysed for their surface structure and utilised in the preparation of form-stable phase change material. The biochar derived from softwood was found to have a superior porous structure with a surface area of 441 m^2/g compared to wheat straw. Biochar and phase change material Rubitherm 28 (RT28) were blended at various wt% and tested for leakage. The composite with 50 wt% of softwood biochar and RT28 had the lowest leakage rate. The developed green phase change-bio composite with minimum leakage has been thoroughly evaluated for its chemical and thermal properties. The latent heat of fusion has been found to be 228.6 J/g, 132.3 J/g and 51.6 J/g, for the RT28, softwood biochar composite, and wheat straw biochar composite respectively. Thermal conductivity was also higher for the composites than that of RT28. The thermal cycling reliability is suitable for thermal storage applications as there is a minimal alteration in the thermal properties observed after 200 cycles. The melting enthalpy of the new and aged composites after 200 cycles has been found to be 136.6 J/g and 132.42 J/g, respectively. The composite with minimal leakage and high thermal conductivity can potentially revolutionise the area of low temperature latent heat storage. The properties of the form-stable phase change-bio composite synthesised in this work make it suitable for application in the field of thermal management of photovoltaic modules, electronic devices, and buildings.

1. Introduction

The adoption of renewable energy is crucial in the face of global climate change. While electricity generation is often the focus, heating makes up almost half of worldwide final energy consumption and greenhouse gas emissions. Industrial processes use 53 % of energy for heat, followed by 44 % for space heating and hot water in buildings. The demand for energy for space heating, refrigeration, food storage, and thermal energy has increased in recent decades. Renewable heat consumption is expected to increase by almost one-third by 2027. Thermal energy storage (TES) systems can reduce the gap between energy supply and demand, which is essential for the effective use of renewables. The global market size of TES is forecasted to triple by 2030, growing to over 800 GWh by 2030. Investments in TES applications, particularly for cooling and power, could reach between United States Dollar (USD)13 billion and USD 28 billion in the same timeframe [1].

Among the available energy storage options (i.e., sensible, latent, and chemical), latent heat is practical from the perspective of energy storage density, compatibility with other materials, and cost. Latent heat storage utilises Phase Change Material (PCM), which absorbs and

Abbreviations: AWSB, Activated Walnut Shell Biochar; BET, Brunauer-Emmett-Teller; CLP, Carbonized Lemon Peel; DSC, Differential Scanning Calorimetry; FESEM, Field Emission Scanning Electron Microscope; FTIR, Fourier-transform infrared; HD, Heptadecane; MP, Methyl Palmitate; PCM, Phase Change Material; PVC, Polyvinyl Chloride; RT28, Rubitherm 28; TES, Thermal energy storage; TG, Thermo Gravimetric; USD, United States Dollar; WSB, Walnut Shell Biochar; XRD, X-ray powder diffraction.

* Corresponding author.
E-mail address: Manosh.Paul@glasgow.ac.uk (M.C. Paul).

https://doi.org/10.1016/j.est.2024.110995
Received 30 October 2023; Received in revised form 15 January 2024; Accepted 15 February 2024
Available online 23 February 2024

releases energy during phase transition. The growing PCMs market, which is approximately USD 1.9 billion and expected to increase at an annual rate of more than 17.4 % in the coming years, has been fuelled by advances in material research [2]. The use of PCMs in latent heat storage systems has proved to be an efficient means of utilising the heat from solar energy and industrial waste, but it also shows promising applications in emerging areas such as smart fabrics, biomedical, and electrical cooling. Growing interest in PCM can be observed from the exponential rise in publications and patents published in this area [3]. Some advantages associated with PCM include their ability to offer adjustable phase change temperatures, significant heat absorption during fusion, inert chemical properties, substantial storage capacity, absence of phase separation, inherent nucleation capability, and reduced vapor pressure when undergoing melting. However, PCMs also exhibit certain limitations such as having relatively lower thermal conductivity as well as changes in volume during phase transitions, which subsequently elevate thermal resistance during the phase shift procedure [4]. As a result, it is imperative to improve the thermophysical properties of PCMs to achieve efficient thermal energy storage [5]. With the aim of improving thermal characteristics and avoiding leakage from volume expansion, researchers have developed an innovative solution: forcing PCM into a porous material held in place by capillarity. Minerals, polymers, metal foams and carbonaceous porous materials are some of the most researched supporting matrixes to hold the PCM from leaking and improve their thermal properties [6].Compared to other supporting materials, biomass-derived biochars are low in price and have a high PCM loading capacity, and therefore are more in line with the needs of sustainable development [7]. The abundance and replenishment nature of solid biomass prompt use of biochar as a renewable substitute for the synthetic supporting material in developing form-stable PCM composite [8]. Biochar is produced through slow pyrolysis process, which involves heating biomass in the absence of air [9].

A host of works has been carried out to develop form-stable green PCMs with biochar as a supporting material. Bordoloi et al. [10] have successfully prepared and characterized PCM composites with biochar derived from sugarcane bagasse, water hyacinth and yellow oleander. Binary and ternary blends of these biochars have also been explored. The pore structure of biochar was found to be mesoporous and suitable for confining the PCM during phase transition within its pores. Among the various samples studied, the form-stable PCM composite produced with a binary blend of water hyacinth and sugarcane bagasse as a supporting matrix provided the maximum value of latent heat of fusion, i.e., 98.8 J/g. The same group of researchers also developed form-stable PCM with water hyacinth biochar for various solar energy applications such as crop drying and cooling of photovoltaic-thermal collector [11,12]. Biochar generated from waste walnut shells by pyrolysing at 500 °C in a nitrogen atmosphere has been used as a supporting matrix for Methylene palmitate (MP) [13]. The researchers further activated the biochar and used it for form-stable composite preparation.

The composite produced with Activated Walnut Shell Biochar (AWSB) showed an enhancement in fusion enthalpy of 27.5 % compared to that of the composite prepared with Walnut Shell Biochar (WSB). However, the thermal conductivity was observed to be 1.58 and 1.9 times higher than Methyl Palmitate (MP) when AWSB and WSB were used as a supporting matrix in the composite, respectively [13]. Carbonized Lemon Peel (CLP) blended with n-Heptadecane (HD) at 60 % wt. showed no leakage [14]. The composite had a latent heat storage capacity of 141.8 J/g with a 77 % higher thermal conductivity than that of HD. Form-stable PCM based on delignified wood flour and myristyl alcohol was also found suitable for constructing composite boards with immense potential in building thermal management [14,15]. Gu et al. [16] developed and studied a form-stable PCM made of carbonized pepper straw and Palmitic acid. The composites were observed to remain stable after 100 cycles of melting and solidification. Besides biochar, three-dimensional hierarchical porous carbon has also been investigated as a potential supporting matrix for developing form-stable and highly conductive thermal energy storage materials [17,18]. Composite prepared of polyethylene glycol and 3-D porous carbon derived from porous polyacrylonitrile showed a high energy density of 173.5 J/g and reported a ten-fold improvement in thermal conductivity as compared to pristine polyethylene glycol [17]. Form-stable phase change material has been successfully synthesised by Lv et al. [19], with waste phoenix leaf biochar as a supporting matrix for the three most used organic PCMs (paraffin, stearic acid, and polyethylene glycol) by the vacuum impregnation method. The authors observed that pyrolysis temperature is directly related to the thermal conductivity of the composite PCM and has better thermal stability.

As reported in the literature reviewed, biochar produced from waste agricultural biomass and softwoods is very few. In this work, biochar derived from softwood and wheat straw is investigated as supporting material. This work is also an attempt to present a comparative study of biochar derived from herbaceous and wood-based feedstock for their applicability in development of form stable phase change material. Wheatstraw is generally burned by farmers in most countries after harvest creating a nuisance of huge amounts of greenhouse gas emissions. Thus, a sustainable way of managing vast volume wheatstraw generated post-harvest is pyrolysing it to biochar. Wheatstraw biochar has been explored for containing organic paraffin in its porous network. Given the beneficial attributes of biochar possessing unique thermophysical properties, it is worthwhile to investigate its potential combination with PCMs and its implications for thermal storage capabilities. Biochar-RT28 composites at varying mass proportions (90:10, 80:20, 70:30, 60:40 and 50:50) were prepared using a simple impregnation method, and a leakage test was carried out. Followed by the identification of leakproof samples, these were thoroughly characterized for chemical and thermal properties. From the application point of view, the thermal stability of PCM is an important parameter. Sustaining key attributes like heat storage capacity, thermal conductivity, and phase change temperatures over extended periods of usage holds significant importance. In this work, therefore, 200 cycles of charging and discharging have been carried out to test the thermal stability. The thermal behaviour of the material during charging-discharging has been studied experimentally. This work will be useful for future research on numerical modelling and latent heat system design.

2. Methods and materials

2.1. Preparation of RT28-biochar composite PCMs

The creation of nanometer-scale pores during biomass pyrolysis is largely attributed to the vaporisation of organic compounds. Hemicellulose and cellulose decomposition occur within the temperature bracket of 200–400 °C, whereas lignin exhibits a more intricate structure and complex degradation mechanisms [20]. Lignin decomposition predominantly occurs within the temperature span of 350–500 °C, gradually persisting until reaching 900 °C. Therefore, biochar used as a supporting material in the current study has been produced at 700 °C to ensure a high degree of carbonisation and therefore to provide a well-developed pore network. The biochar was produced in a pilot-scale rotary kiln pyrolyser at the United Kingdom Biochar Research Centre (University of Edinburgh). Further details on the production process can be found in [21]. The hydrogen-to-carbon molar ratio (H:C ratio) serves as a straightforward indicator of both aromaticity and carbon stability. A higher H:C ratio suggests enhanced carbon stability and resistance to decomposition in biochar, particularly in graphitic structures devoid of hydrogen (or oxygen). As presented in Table 1, H:C ratio is below 0.4, which is indicative of the high carbon stability of the biochar [22]. Another advantage of selecting high pyrolysis temperature is to obtain combustion-resistant biochar with no volatiles clogged in its pores [23]. The strong C—C covalent bonds in high-temperature biochar are also responsible for greater fire resistance.

RT28 (PCM) and biochar were separately weighed in a precise

Table 1
Characteristics of wheat straw and softwood biochar.

	Wheat straw	Softwood
C_{total} (wt% dry basis)	69.04	90.21
H (wt% dry basis)	1.18	1.83
H:C_{total} (Molar ratio)	0.2	0.24
O (by difference) (wt% dry basis)	5.3	6.02
Total ash (wt% dry basis)	23.82	1.89
Total N (wt% dry basis)	1.32	0.1
pH	10.03	8.44
Electric conductivity	1.52	0.16

laboratory scale for composite preparation. Initially, RT28 is put in a glass beaker and placed inside the hot air oven (Memmert UF30) maintained at a temperature of 35 °C. Once the RT28 transits to a liquid phase completely, biochar is slowly introduced into the molten PCM and vigorously stirred with a stirrer for 5 min. The mixture is kept in the hot air oven for 16 h with intermittent stirring. After removing the composite from the oven, it is allowed to cool to room temperature. The obtained mixture is referred to as a form-stable composite PCM, and denoted as C90/10, C80/20, C70/30, C60/40 and C50/50. Then, the composites were used for further characterization. Fig. 1 shows the steps of preparing the form-stable composite by the simple impregnation method [12].

2.2. Characterization techniques

Surface morphologies of the materials are assessed using a Field Emission Scanning Electron Microscope (FESEM) (Manufacturer: Zeiss, Model: Sigma). The biochar's surface area, pore size, and pore volume are determined using a Brunauer-Emmett-Teller (BET) surface area analyser (Quadrasorb EVO/SI). Crystallinity and phase changes are examined using X-ray powder diffraction (XRD) (Rigaku MiniFlex benchtop (A4-19) diffractometer) equipped with Cu-sealed tube X-ray sources. XRD measurements are conducted with a 10° step size within a two-theta degree range of 10° to 70° while scanning the samples. The identification of functional groups and chemical compatibility between the PCM and the supporting materials in the composite was accomplished through Fourier-transform infrared (FTIR) spectroscopy, utilising a JASCO Fourier Transform infrared spectrometer measurement system. The spectral analysis was conducted across the wavenumber range of 600–4000 cm^{-1}. Thermal stability is evaluated employing a high-temperature Thermo Gravimetric (TG) System (TA Instrument, SDT Q600 V8.3) with a heating rate of 10 °C/min, spanning from 20 to 1000 °C under an Argon atmosphere. Differential Scanning Calorimetry (DSC) experiments are executed using the TA Instruments DSC 25, accompanied by the RCS90 refrigerated cooling system, employing a heating rate of 10 °C/min over a temperature range of −10–95 °C. During DSC analysis, purging is carried out using pure nitrogen gas. A cycling stability assessment of the optimal biocomposite PCM, coupled with an analysis of the solidification process, is performed utilising the aforementioned DSC equipment. This is done with a heating rate of 10 °C/min within a temperature range of 20–60 °C. For measuring thermal conductivity, the Hukesflux, TPSYS20 thermal conductivity meter is employed, featuring a TP08 needle probe. The meter offers a measurement range of 0.1 to 6.00 W/mK.

2.3. Form stability and leakage test

Each sample was cast into a cylindrical pellet of diameter 10 mm and height 2 mm. The respective initial mass, M_o was measured using a precise analytical balance. The composites were placed on a filter paper, at a temperature of 35 °C inside a hot air oven for 30 min. The sample has been taken out of the oven and mass, M_t, was measured. The leakage rate or mass loss of PCM can be calculated as [25].

$$L = \left[\frac{M_o - M_t}{M_o}\right] \times 100\% \quad (1)$$

2.4. Evaluation of photo-thermal conversion performance

The composite material and the pure PCM are positioned within cylindrical enclosures with the top surface open for radiation flux and then subjected to irradiation under a halide lamp. The radiation intensity is validated using a radiometer. Once the temperature of each block reaches a specific threshold, the simulated solar light source is

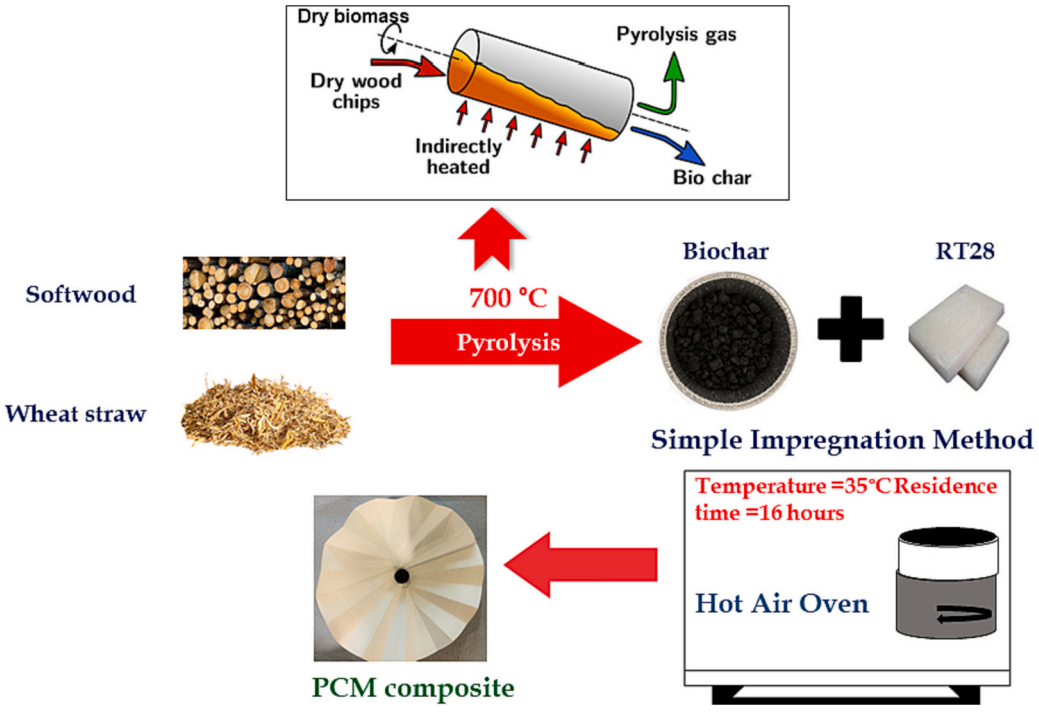

Fig. 1. Steps in preparation of PCM composite from biochar and RT28 [12,24].

switched off, permitting natural cooling. The temperature fluctuations of each composite block are monitored and recorded using a data logger, as illustrated in Fig. 2. The efficiency of solar-thermal energy conversion, denoted as η_{st} can be computed using the subsequent equation [26],

$$\eta_{st} = \frac{m\Delta H_m}{GA(T_o - T_f)} \quad (2)$$

where m is the mass of the PCM composite sample, ΔH_m is the melting enthalpy of the composite, G is the light intensity of the simulated sunlight, A is the area of the sample exposed to the radiation, and T_o and T_f are the time of the start and end of phase transition, respectively. In this work, a cylindrical container made of Polyvinyl Chloride (PVC) with a diameter of 5 cm has been used to hold the sample. The intensity value of simulated irradiation of 200 mW/cm^2 is used. Sample mass of 5 g, 3 g and 3 g is used for RT28, C_{WS}50/50 and C_{Sw}50/50, respectively.

3. Results and discussion

After carrying out various analyses to find the physical, chemical, and thermal characteristics of the developed form-stable PCM composites using the standard instruments and methods, a comprehensive discussion is put forward in this section.

3.1. Form stability and leakage tests

Our findings showed that as the fraction of biochar in the composite increases, the form stability improves and leakage reduces. Observation of the filter paper through visual inspection has revealed the escape of PCM from the biochar matrix during the melting process as shown in Fig. 3 and quantified it as presented in Fig. 4. When 50 wt% of the composite is biochar, it provides the lowest leakage. A higher proportion of biochar in the composite provides more pore sites for the PCM to settle into and hold on to the pores by capillarity. The sample composition (PCM/biochar) with minimum leakage. i.e., C50/50 is selected for further characterization. The leakage is 7.9 % and 2.7 % for wheat straw biochar composite and softwood biochar composite, respectively.

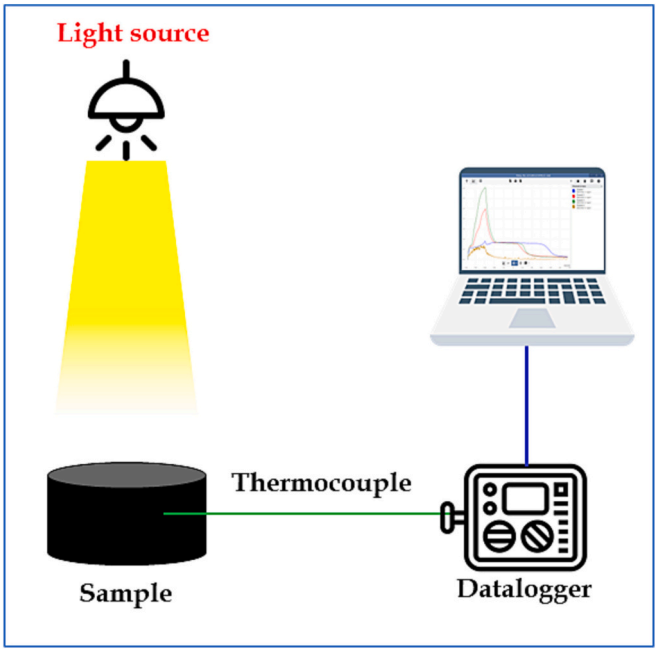

Fig. 2. Experimental setup for estimation of photothermal conversion.

3.2. Morphology, surface area and porosity

As seen from the SEM images presented in Fig. 5, the biochar particle has lots of pores on its surface. The SEM image for the PCM composite confirms that the pores on the biochar particle have been filled with PCM. Numerous pores can be observed on the surface of the wheat straw biochar to form a net-like structure in Fig. 5(a). As can be seen in Fig. 5 (c), the pore structure on softwood biochar is more organised, and no deposition of broken skeletal material is observed. These pores are filled with RT28 after the impregnation process is completed, Fig. 5(b) and (d). The pore arrangement on the biochar surface is more organised in the case of softwood than that of wheat straw. In wheat straw, some broken skeletal material is observed to be settled in the pores, thus reducing the effective pore volume and surface area available for the accommodation of phase change material.

Characterizing biochar samples with a prevalence of microporosity, particularly those featuring small micropores, presents difficulties in N_2 adsorption analysis. These challenges arise primarily due to the lower measurement temperature (77 K), which leads to heightened limitations in intra-particle transport and potential pore deformation. Consequently, there is a tendency for biochar microporosity to be underestimated in such cases. Fig. 6(a) and (d) show the N_2 absorption-desorption isotherm for wheat straw and softwood; the isotherms are open hysteresis, which is due to the non-equilibrium conditions. The main reasons for the occurrence of the open hysteresis N_2 isotherm in biochar can be attributed to the complex porous structure, capillary condensation, pore blocking and surface chemistry [20,27]. Biochar possesses a complex porous structure, consisting of micro-pores, meso-pores, and sometimes macropores. These pores can have different shapes, sizes, and connectivity. During adsorption, nitrogen molecules can enter these pores and get trapped on the internal surfaces of biochar. Capillary condensation occurs when the pressure decreases during desorption, and nitrogen molecules get trapped in the narrow necks or capillaries of the porous structure due to capillary forces. These trapped molecules remain adsorbed even at lower pressures, causing the desorption branch not to overlap with the adsorption branch. In some cases, larger molecules or aggregates of nitrogen may enter the pores during adsorption and block the entrances of the pores. When the pressure is reduced during desorption, these larger aggregates may not be easily removed, leading to non-overlapping hysteresis loops. The surface chemistry of biochar, including functional groups and surface polarity, can influence the adsorption and desorption behaviour of nitrogen. Surface interactions may result in the preferential adsorption at specific sites, affecting the shape of the hysteresis loop.

Throughout the pyrolysis process, breakdown of the carbon matrix and the concurrent liberation of volatile components contribute to the emergence of pores, primarily in the nanometer range. This subsequently gives rise to the establishment of the porous structure inherent to biochar. The surface areas calculated from the multi-point BET plots for wheat straw and softwood biochar, as shown in Fig. 6(c) and (f), are 170 m^2/g and 441 m^2/g, respectively. Softwood biochar has an almost 2.6 times higher surface area as compared to wheat straw biochar; this is because of the higher lignin content in woody biomass feedstock. Another reason is the obstruction of micropores due to the migration and sintering of inorganic elements in biochars from agricultural biomass, which can be clearly seen from the SEM images of biochars [28]. Table 2 presents various surface parameters and porosity information about the biochars analysed in this study. Pore diameters of both biochars fall within the microporous range with a slightly higher value in the case of wheat straw biochar than that of softwood biochar.

3.3. Crystallization characteristic and chemical properties

The functionality of the supporting matrix, pristine PCM, and composites was examined through FTIR spectra analysis within the wavelength range of 600–4000 cm^{-1}. Figs. 7 and 8 show the chemical and

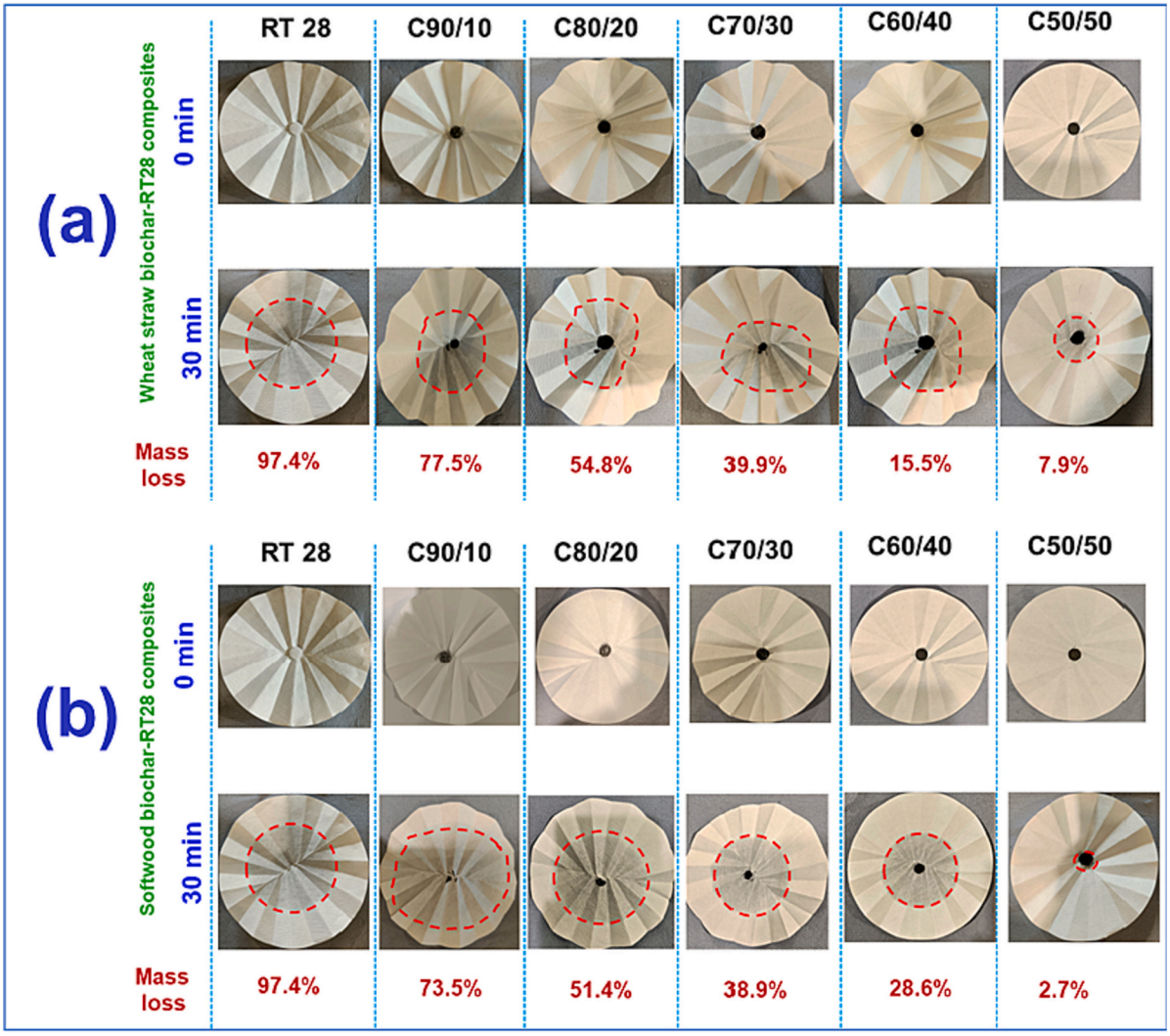

Fig. 3. Leakage test of RT28 and PCM composite samples, (a) Wheat straw biochar-RT composite; (b) Softwood biochar-PCM composite.

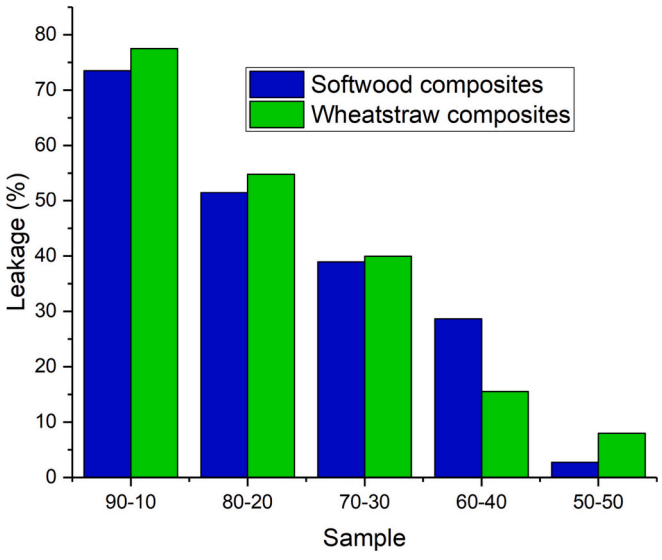

Fig. 4. Extent of melting for different composite samples during leakage test.

crystallization characteristics of biochar, PCM and composites, respectively. The notable absorption peaks evident in both the supporting materials and RT28 within the composite PCMs signify the physical integration of pristine PCMs into the biochar pores. In the case of the FTIR spectra of softwood biochar, aromatic peaks were observed around 1500–1600 cm^{-1} due to the stretching vibrations of aromatic carbon-carbon double bonds present in lignin-derived compounds. As observed from the FTIR plots, the characteristic absorption peak of wheat straw biochar is located at 1060 cm^{-1}, which is the stretching vibration of C—O. This is attributed to cellulose, hemicellulose and lignin since the biochar has been produced from an herbaceous feedstock. Importantly, physical adsorption encompasses the mechanisms like capillary forces, Van der Waals interactions, and π-π electron donor-acceptor interactions occurring between PCM molecules and the biochars [29]. The composite PCMs showed all the characteristic absorption peaks of the PCM including the noticeable peaks of hydrocarbon absorption bands. No new absorption peaks were monitored. This observation signifies that the supporting materials uphold the crystalline structure of RT28 without generating a novel chemical group. This preservation is essential to ensure the phase transition of the prepared composite PCM during thermal storage. A C═C stretching peak was evident around 1480 cm^{-1}, while the weak peaks at 740 cm^{-1} were attributed to C—H vibrations on the carbon ring. The pristine PCM exhibited pronounced absorption peaks corresponding to the symmetric and asymmetric stretching vibrations of methylene (2952 cm^{-1}) and methyl (2846 cm^{-1}), as well as the C—H symmetric and bending

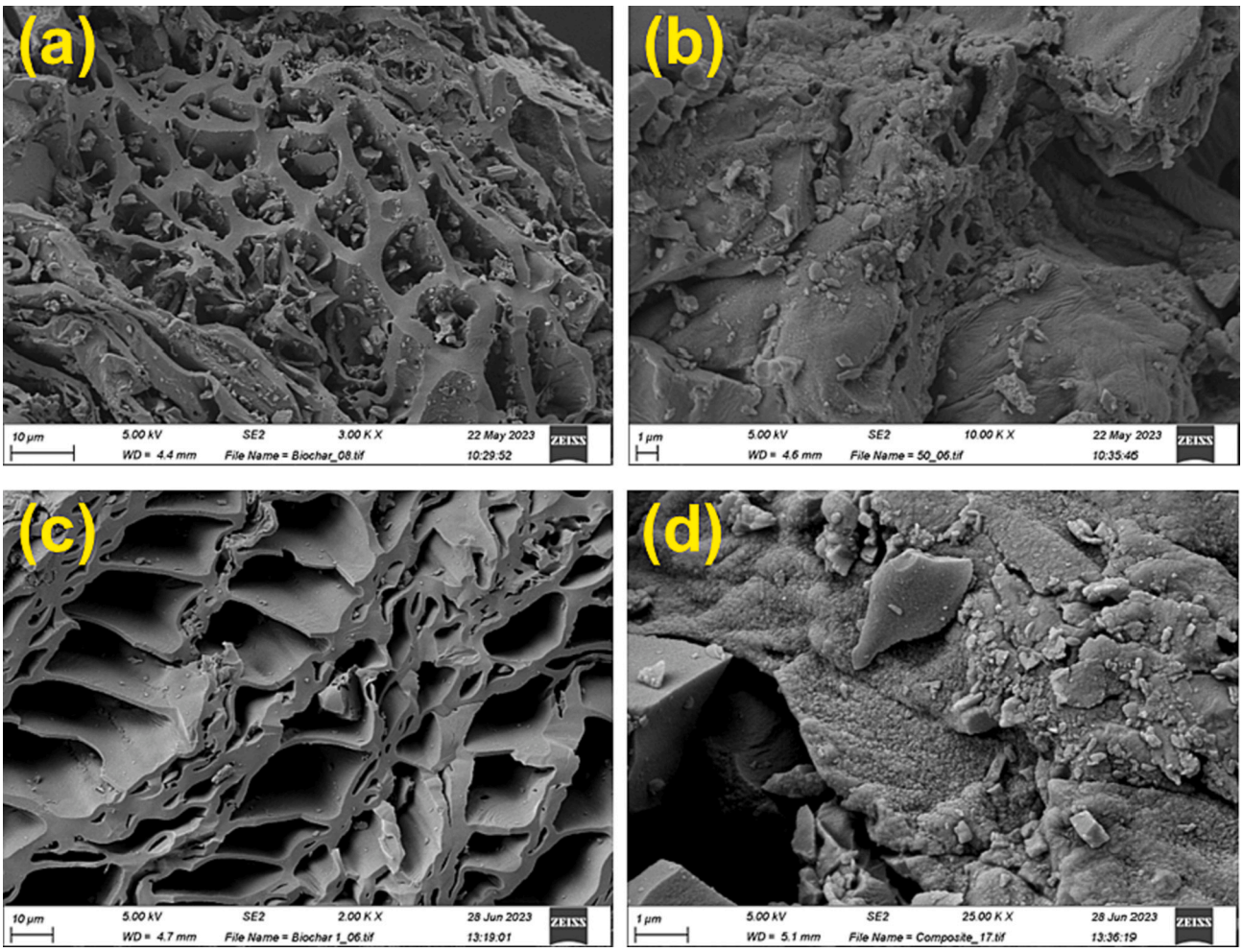

Fig. 5. SEM image of, (a) Wheat straw biochar; (b) Wheat straw biochar-RT composite (C_{WS}50/50); (c) Softwood biochar; (d) Softwood biochar-PCM composite (C_{SW}50/50).

deformation bands at 1377 and 1464 cm^{-1}, respectively. The absence of any new peaks confirms the successful impregnation of the pristine PCM into the porous biochars.

Broad peaks in the wheat straw biochar are attributed to the amorphous component, while the presence of sharp peaks at 38° and 44.3° confirms the presence of crystalline components. Whereas, as can be seen from Fig. 8(b), only sharp peaks (38.3° and 44.57°) are displayed in the XRD plot of the softwood biochar, confirming its crystalline nature. This is due to the higher carbon percentage in the biochar, which is above 90 %. The composites prepared with both the biochars as supporting materials display the sharp peaks, indicating their crystalline nature. The position of the peaks is at the same angle as that of RT28. The peak intensities observed in the composites are diminished compared to those of the pure PCM. This occurrence can be attributed to the fact that diffraction patterns of moisture absorbing PCMs are less distinct within the biochar, resulting in a broader pattern with peaks of lower intensity. This effect is likely due to the porous structure, which facilitates the return of the absorbed liquid to its initial state within the cavities [30].

3.4. Thermal properties

3.4.1. Thermal stability

Thermal stability is an important study for confirming the operational limit of the composite PCM. As shown in Fig. 9, the RT28, wheat straw biochar, softwood biochar, wheat straw biochar composite (C_{WS}50/50) and softwood biochar composite (C_{SW}50/50) showed one-step thermal degradation with maximum weight loss occurring at approximately 110 °C, 75 °C, 46 °C, 140 °C and 147 °C, respectively. Thermal degradation continues until 240 °C for RT28 with almost 99.2 % of mass loss. While for C_{SW}50/50 and C_{WS}50/50 the single-step degradation continues until the temperature of 232.5 °C and 222.7 °C, having a mass degradation of 62.5 % and 44.4 %, respectively.

The thermal degradation starts gradually after the temperature crosses 120 °C and reaches a maximum value of 2.62 %/°C at 233 °C in the case of pure RT28 as shown in Fig. 9(c). Whereas for the C_{WS}50/50 and C_{SW}50/50, the maximum degradation rates of 1.13 %/°C and 1.71 %/°C are observed at 213 °C and 225 °C respectively. The rate of decomposition in the composites is slower compared to that of pure paraffin. This phenomenon is likely attributed to the robust intermolecular interaction between the functional biochar pore structure and RT28, which further contributes to the stability preservation. Furthermore, the substantial presence of micro- and meso-pores in the biochars generates an effective capillary force, thereby upholding thermal stability and enhancing the shape of PCMs within the synthesised composites. Unlike its impact on energy storage capacity, the incorporation of RT28 into the biochar demonstrates satisfactory thermal stability, meeting the necessary criteria for practical applications.

3.4.2. Energy storage capacity

Material's capability of storing and releasing heat is directly linked to phase change temperature and enthalpy of phase change [31]. The

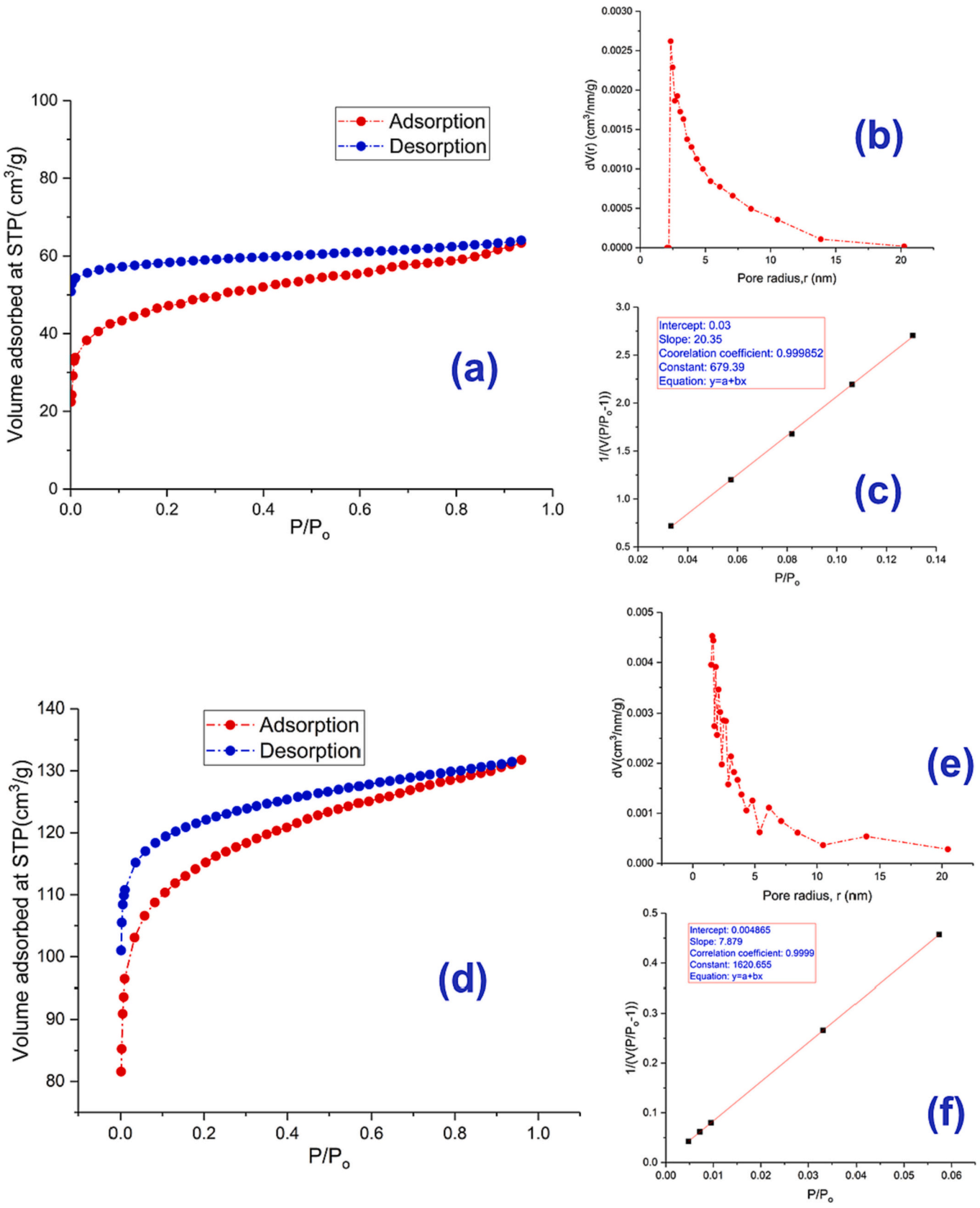

Fig. 6. Structural characterization of biochar, (a) the nitrogen adsorption–desorption curve of wheat straw biochar; (b) pore size distribution curve of wheat straw biochar; (c) Multi-point BET curve of wheat straw biochar; (d) the nitrogen adsorption–desorption curve of softwood biochar; (e) pore size distribution curve of softwood biochar; (f) Multi-point BET curve of softwood biochar.

Table 2
Surface parameter and porosity of the biochars.

	Surface area (m^2/g)	Pore diameter (nm)	Pore volume (cm^3/g)
Wheat straw	170	1.9	0.011
Softwood	441	1.5	0.017

thermal properties such as melting temperature, melting enthalpy, solidification temperature, and solidification enthalpies of the pristine RT28 and biochar-RT28 composites were evaluated by DSC analyses.

The melting temperature of the form-stable composites, as observed in Fig. 10, is slightly higher than that of pure RT28, and conversely, the solidification temperature is lower for the composites. The melting temperatures for RT28, $C_{SW}50/50$ and $C_{WS}50/50$ are found to be 24 °C, 25.4 °C and 25 °C, respectively. While the solidification temperature is 25.6 °C, 25.2 °C and 25 °C for RT28, $C_{SW}50/50$ and $C_{WS}50/50$, respectively. The variation trend in the melting point of the composite with respect to the pristine PCM can be explained with the aid of the Clausius-Clapeyron relation [32,33], which is expressed as follows:

$$ln\left(\frac{T_{m,composite}}{T_{m,pure\ PCM}}\right) = \left(\frac{\Delta V_m}{\Delta H_m}\right) \times (P_2 - P_1) \quad (3)$$

where, $T_{m,composite}\ (K)$ and $T_{m,pure\ PCM}(K)$ represent the phase transition temperature of the form-stable composite and pure PCM respectively, $\Delta V_m(m^3)$ and $\Delta H_m\left(J/g\right)$ are the volume change of the material and phase change enthalpy respectively. $P_1(MPa)$ and $P_2(MPa)$ represent the ambient pressure during the process of phase change. The volume of the pure PCM increases in the crystal structure of the carbonaceous biochar (ΔV_m>0) and ambient pressure will also increase due to restriction of the crystal structure, thus shifting the melting temperature of the compos-

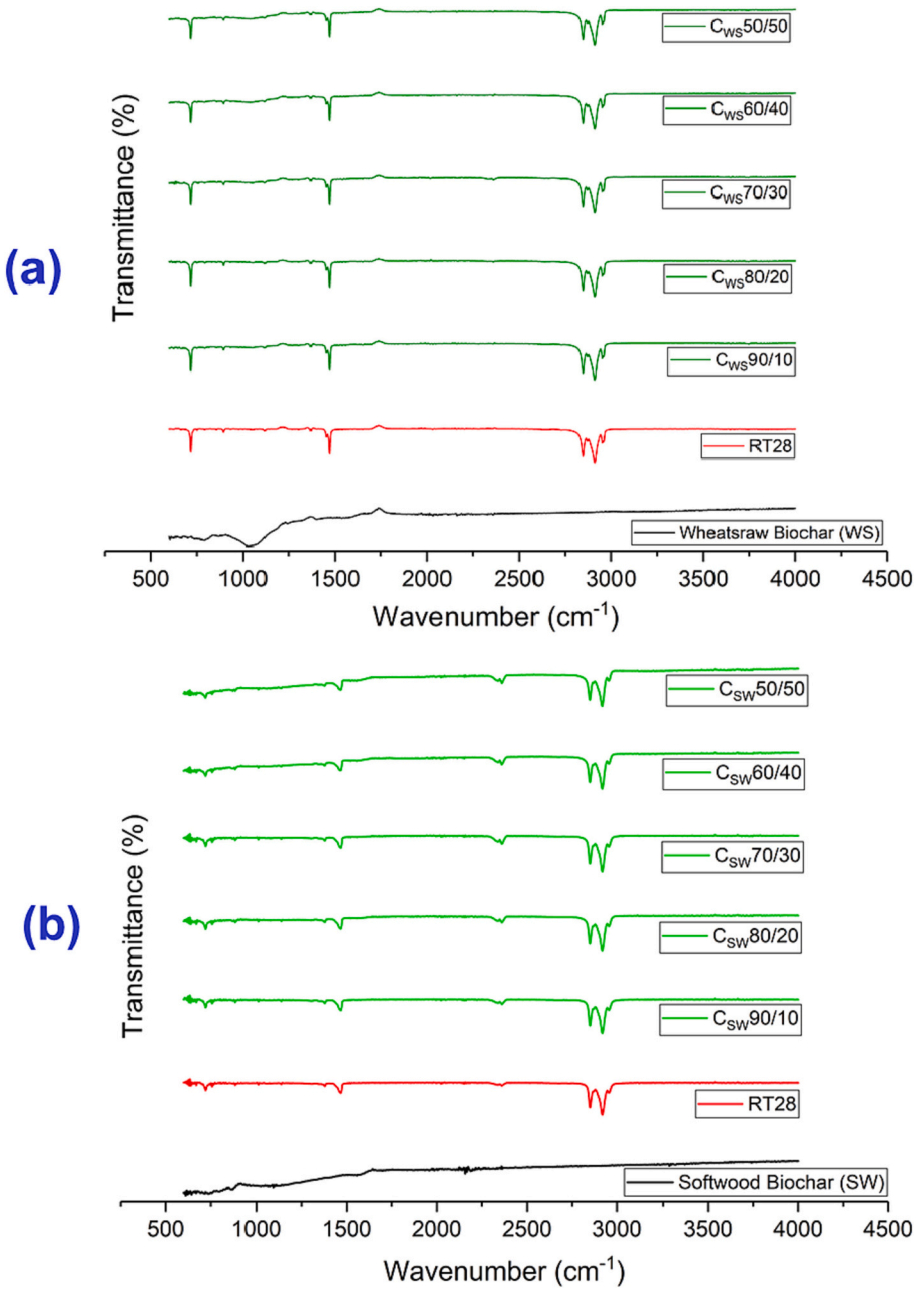

Fig. 7. FTIR plots of biochar, RT28 and PCM composites prepared with different RT/biochar mass ratios, (a) Wheat straw biochar-RT composite; (b) Softwood biochar-PCM composite.

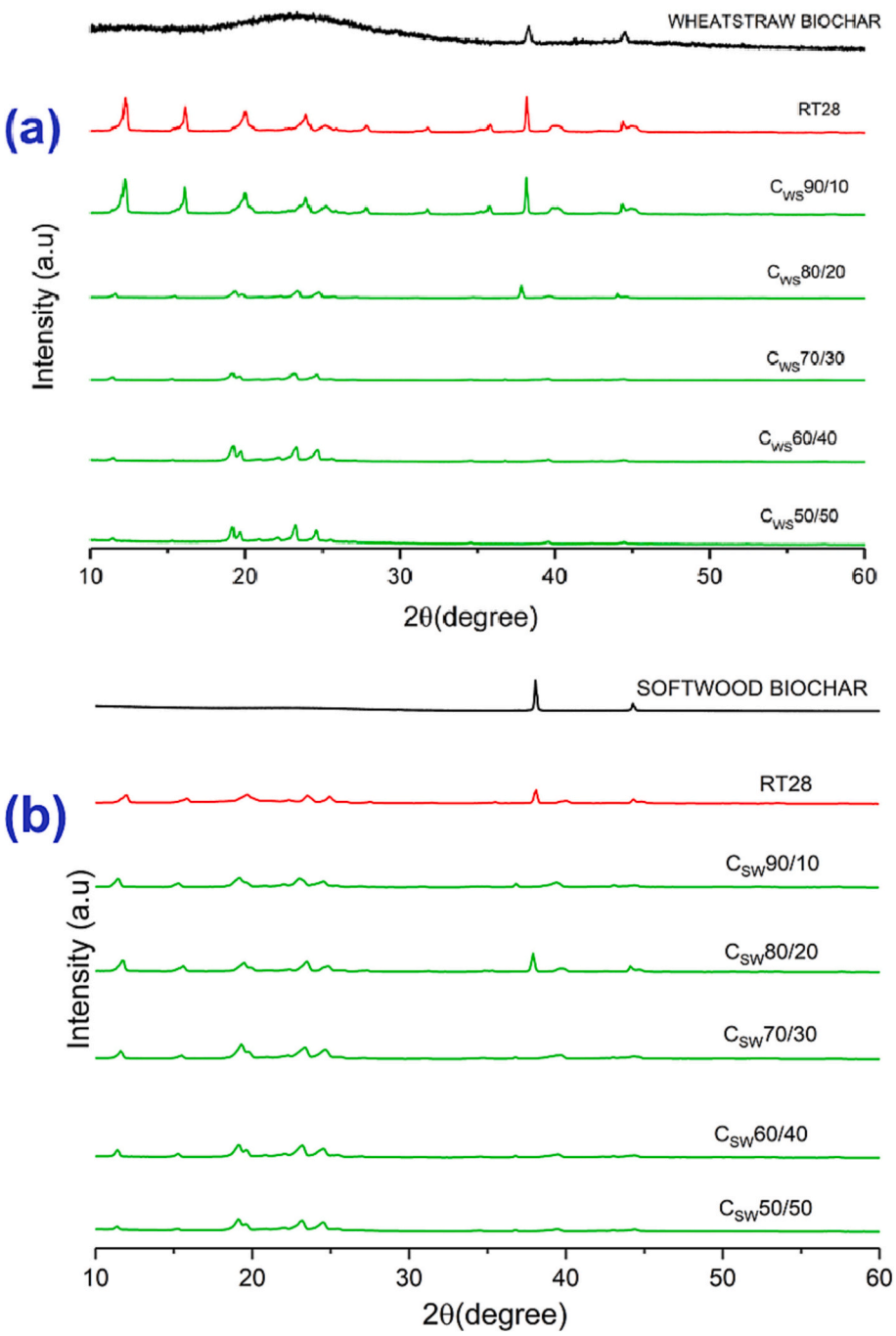

Fig. 8. X-ray diffraction patterns of biochar, RT28 and PCM composites prepared with different RT/biochar mass ratios, (a) Wheat straw biochar-RT composite; (b) Softwood biochar-PCM composite.

ites to higher value. This phenomenon is referred to as "Melt Bilge Response".

The values of phase change enthalpies are found to be lower than the transition enthalpy of pristine PCM. The heat of fusion, as obtained from the DSC curve shown in Fig. 10(a) for the RT28, C_{SW}50/50 and C_{WS}50/50, is 228.6 J/g, 132.3 J/g and 51.6 J/g, respectively. The composites have a lower value of phase transition compared to the pure PCM. It is mainly due to the presence of carbonaceous biochar in the composite, which does not undergo any phase transformation during the heat absorption process and the pores within the biochar impede the typical molecular mobility of PCM molecules as they undergo phase transition, thereby reducing the heating enthalpy [29].

Comparing form-stable PCM composites based solely on the latent heat of fusion is ambiguous due to various parameters such as support matrix load ratio, PCM properties, and synthesis process. Thus, Table 3 presents a comparison of these composites with those found in the literature based on the percentage reduction of latent heat of fusion in the base PCM while taking these parameters into account. The comparison shows that the form-stable composite made by impregnating softwood biochar with RT28 has a favourable energy storage capability. The reduction in heat of fusion for the softwood biochar-RT28 composite is lower as compared to the other works presented in the table. This is due to the high surface area of the biochar which leads to a higher loading ratio of the RT28 in its pores. The high latent heat of the composite is significant for the application which demands the absorption of a huge quantity of thermal energy.

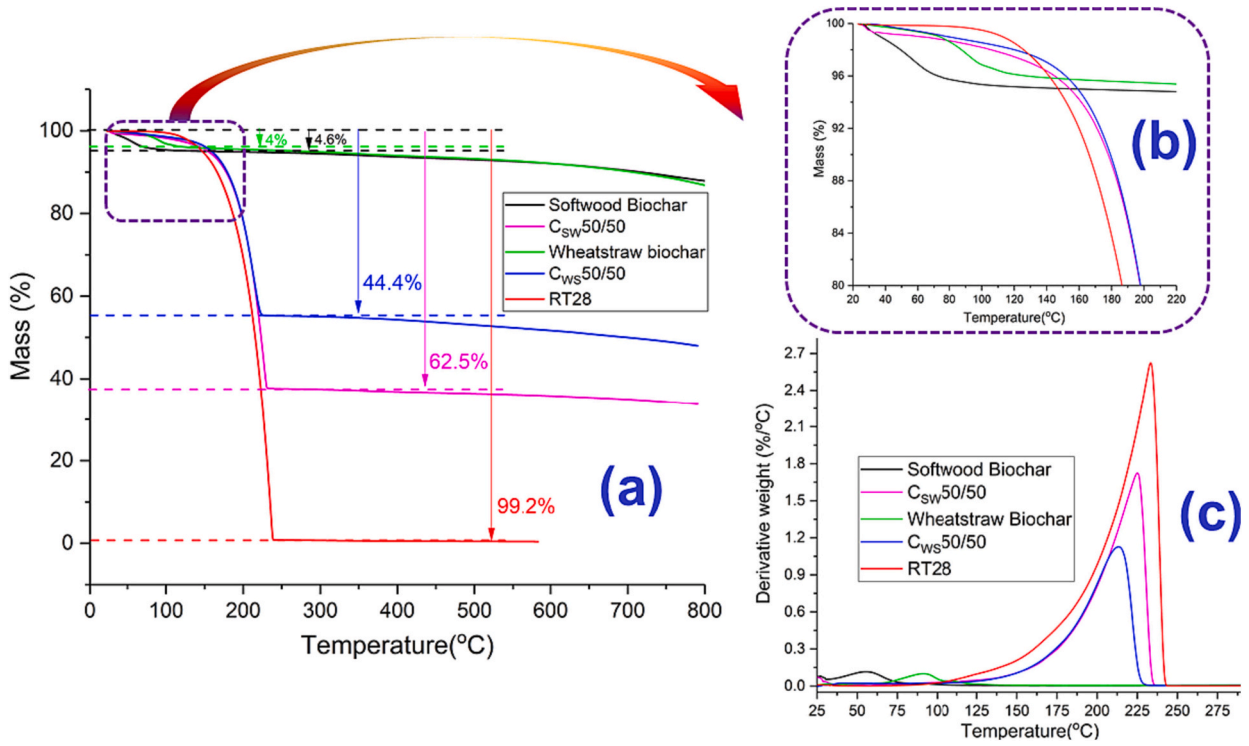

Fig. 9. TGA curves of biochar, RT28 and Wheat straw composites, (a) Thermogravimetric analysis; (b) Zoom out of start of degradation region; (c) Degradation rate variation with temperature.

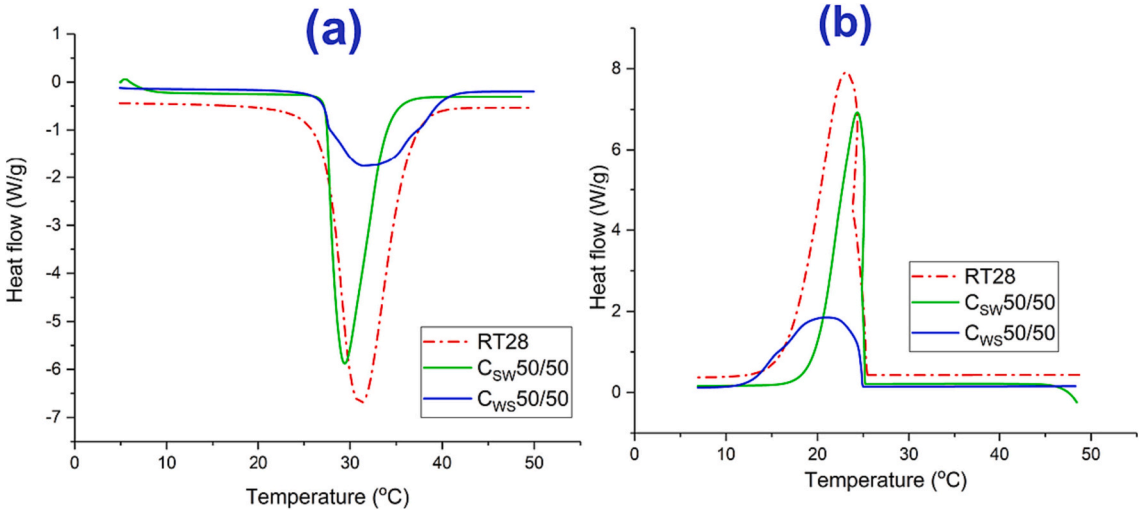

Fig. 10. DSC curves of RT28 and composites (a) melting process and (b) solidification process.

3.4.3. Thermal cycling, reliability, and reversible property of the form-stable composite

A significant concern regarding PCMs is their extended-term stability and dependability, as they tend to degrade over time and lose their storage capacity through prolonged exposure to the surrounding environment and repeated melting and solidification cycles. Consequently, evaluating the cycle test stability of PCMs becomes crucial in order to establish their prolonged durability before integrating them into thermal systems [39]. For studying the effect ageing on thermal properties, 200 melt/freeze cycles have been conducted for the softwood biochar-based composite (C_{SW}50/50). As can be seen in Fig. 11(a) and (b), only a slight change in the melting-solidification curve has been observed after 200 cycles. There is negligible change in the phase transition temperature for the composite at the end of 200 cycles. The melting enthalpy of the new and aged composites after 200 cycles has been found to be 136.6 J/g and 132.42 J/g, respectively. Similarly, the enthalpy of solidification was also found to be altered insignificantly. There is only 3 % and 1 % reduction in the enthalpy of melting and solidification respectively for the aged composite over the new one. Overall, the cyclic test over 200 cycles indicates that the softwood-RT28 composite prepared in this work has outstanding thermal reliability and exhibited a potential value for long-term application.

3.4.4. Thermal conductivity

RT28, C_{SW}50/50 and C_{WS}50/50 are found to have thermal conductivity values of 0.2 W/mK, 0.36 W/mK and 0.25 W/mK respectively. The

Table 3
Comparison of the heat of fusion of form-stable composites developed in this study against those reported in the literature.

Author/ reference	Supporting material	Base PCM	Latent heat of fusion of base PCM (J/g)	Latent heat of fusion of the composite (J/g)	Reduction in latent heat of fusion
Bordoloi et al. [10]	Sugarcane bagasse biochar	OM35	197	91.5	53.55 %
	Water hyacinth biochar	OM35	197	66.6	66.19 %
	Yellow oleander stem biochar	OM35	197	51.39	73.91 %
Hekimoğlu et al. [13]	Walnut shell carbon	Methylene palmitate	255.46	108.32	57.59 %
Atinafu et al. [34]	Bamboo biochar	n-Dodecane	181.6	93.2	48.67 %
Wan et al. [35]	Pinecone biochar	Palmitic acid	219.6	84.74	60.04 %
Mandal et al. [36]	Orange peel biochar	Myristic acid	169.7	67.2	60.40 %
Jeon et al. [37]	Pinecone biochar	Coconut oil	110.4	62.6	43.29 %
He et al. [38]	Water hyacinth biochar	Lauric acid-myristic acid-paraffin	172.37	86.43	49.85 %
Present study	Wheat straw biochar	RT28	228.6	51.6	76.11 %
	Softwood biochar	RT28	228.6	132.3	42.12 %

thermal conductivity of the composites is higher than that of pure RT28 as can be seen in Fig. 12. The carbon network structure of biochar acts as a thermal conductivity matrix to form a heat exchange path, which enhances the thermal bridge effect, and as a result, improves the thermal conductivity of the composites effectively [32].

Table 4 presents various performance parameters of the composites in comparison to the base PCM, which is RT28. The energy storage and discharge and thermal conductivity enhancement in the case of $C_{SW}50/50$ found to be better than those of $C_{WS}50/50$.

3.4.5. Photo-thermal conversion

Fig. 13 shows the light-to-thermal energy conversion curve of RT28, wheat straw biochar-based composite ($C_{WS}50/50$) and softwood biochar-based composite ($C_{Sw}50/50$). The temperature of pristine PCM slowly rose to 29 °C (3355 s) under light irradiation and quickly dropped to room temperature of ~21 °C (19,100 s) after turning off the light source. The temperature-time curve shows a single plateau in the time range of 465–2000 s (temperature range 25–26 °C) for the pristine PCM. In the case of the composites, the length of the plateaus is shorter than that of the pristine PCM. For wheat straw biochar form-stable composite and softwood biochar form-stable composites, plateaus are observed in the time range of 500–710 s and 600–750 s, respectively. After these stable plateaus, the temperature rises in each case. However, the temperature rise is found to be significant in the case of the composites than that of the pristine PCM. The temperature increases and reaches 29 °C, 44.8 °C and 52.3 °C for RT28, $C_{WS}50/50$ and $C_{Sw}50/50$, respectively as seen in the figure.

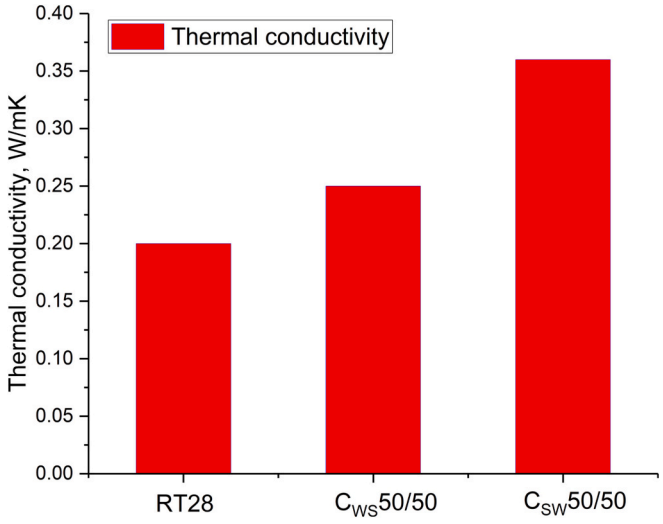

Fig. 12. Thermal conductivity of the composites and pristine RT28.

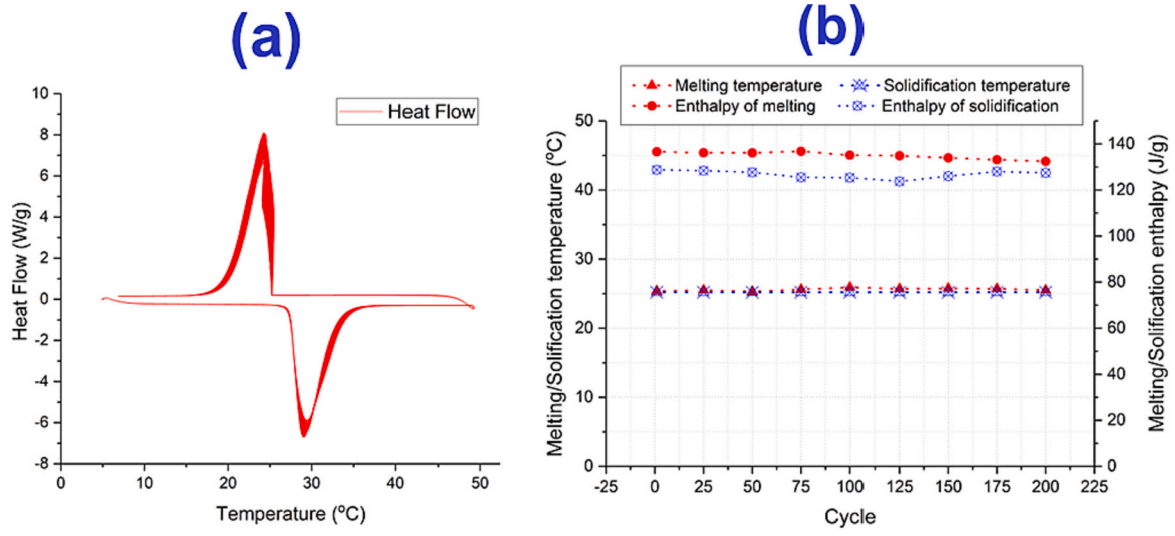

Fig. 11. Thermal cycling and reliability test, (a) DSC curve for 200 melt-freeze cycles; (b) Variation of thermal properties with the number of heating-cooling cycles.

Table 4
Thermal performance parameters of the composites and pristine PCM.

Performance parameter	Wheat straw biochar PCM composite (C_{WS}50/50)	Softwood biochar PCM composite (C_{SW}50/50)
Relative latent heat capacity (R) $= \frac{H_{m.composite}}{H_{m.pure\ PCM}} \times 100\%$	22.6 %	58 %
Actual percentage of energy storage and discharge (E) $= \frac{H_{m.composite} + H_{s.composite}}{H_{m.pure\ PCM} + H_{s.pure\ PCM}} \times 100\%$	25 %	61.4 %
Thermal conductivity enhancement ratio (k*) $= \frac{k_{composite} - k_{pure\ PCM}}{k_{pure\ PCM}} \times 100\%$	25 %	80 %

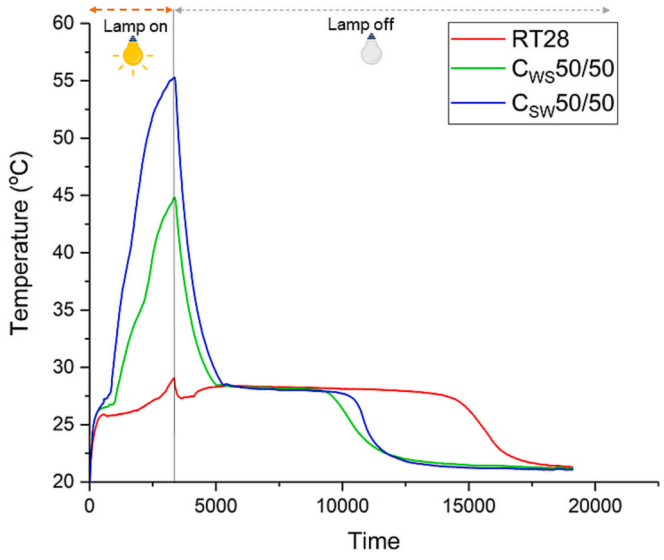

Fig. 13. Photothermal conversion performance curve.

Once the light source was turned off, the temperature dropped rapidly. The temperature reaches 28.5 °C for the composite C_{Sw}50/50 from its peak in 2135 s, whereas for C_{WS}50/50 it took 2370 s to reach 28.3 °C. The phase of rapid temperature plateau corresponding to the phase transition process of solidification was observed for all the samples. During the cooling phase, wider plateau has been observed for C_{Sw}50/50 in the time range of 5500–9700 s compared to the time range of 5600–9000 s for C_{WS}50/50. After the slope region the samples reach reached thermal equilibrium with ambient. The plateau length (time range of approximately 5000–14,000 s) is found to be higher for the pristine PCM than that of the composites.

It can be seen from the Fig. 13, the melting process for RT28, C_{WS}50/50 and C_{Sw}50/50 starts at 305 s, 220 s and 230 s, respectively. The melting continues until 3500 s, 975 s and 850 s for RT28, C_{WS}50/50 and C_{Sw}50/50, respectively. Therefore, the value of photothermal conversion efficiency is evaluated to be 25.5 %, 36.3 % and 62.5 % respectively for RT28, C_{WS}50/50 and C_{Sw}50/50. This outcome illustrates that the composites possess a significantly superior ability to transform solar light energy into latent heat when compared with the pure PCM. This outstanding enhancement in solar photothermal conversion and storage performance is primarily attributed to the substantially heightened sunlight absorption capacity arising from the elevated optical absorptivity of the composite due to black biochar in the composite. These findings strongly imply that the form-stable composite created using softwood biochar, as developed in this study, holds immense potential for utilisation in solar energy applications due to its exceptional photothermal conversion and storage capabilities.

4. Conclusions

In this study, a mixture of biochar and organic PCM (RT28) was successfully created using a simple impregnation method. The biochars used in this study showed suitable surface properties for their applicability as supporting material for form stable PCM development. No chemical interaction occurred between the components, indicating good chemical structure stability in the resulting composite. The composite made with softwood biochar had a higher loading capacity for RT28 due to its larger surface area of 441 m^2/g, and negligible leakage in the composite containing 50 wt% of biochar. The composite made with softwood biochar yielded better results in terms of key parameters such as photothermal efficiency and thermal conductivity.

Key findings from the study include:

1. RT28 was effectively impregnated into the biochar pores with minimal leakage. There was only physical interaction between the PCM and biochar.
2. Thermal stability and phase transition characteristics of the softwood biochar composite (CSW50/50) were satisfactory, with lower phase change enthalpies compared to pristine PCM. The enthalpies of melting for RT28, CSW50/50, and CWS50/50 were 228.6 J/g, 132.3 J/g, and 51.6 J/g, respectively. CSW50/50 showed a reduction in enthalpy of melting of 42.12 % compared to pure RT28, which is comparable to other recent composites.
3. Thermal conductivity increased in the composite compared to pure PCM due to the carbon-rich biochar providing a thermal transport network. An 80 % improvement was observed for CSW50/50 compared to RT28.
4. Photothermal conversion efficiency was 25.5 % and 62.5 % for RT28 and CSW50/50, respectively, indicating a better capability to convert solar light energy into latent heat compared to pure PCM. The composite exhibited 1.45 times more photothermal conversion efficiency as that of pristine RT28, which makes the composite suitable for solar energy applications.
5. There was negligible change in the phase transition temperature for CSW50/50 after 200 cycles, with only a slight reduction in the enthalpy of melting and solidification.

Overall, the form-stable composite created using softwood biochar shows potential for utilisation in solar energy applications. The latent heat capacity of the composite is retained to a reasonable level as compared to existing form stable composites, however there is a scope for improving thermal conductivity by adding chemically compatible highly conductive fillers or additives. There is a requisite of in-depth study on the optimisation of the biochar production parameters to obtain best results in terms of surface area, pore size and pore volume. Co-pyrolysis of variety of biomass feedstocks to obtain biochar of desired pore structure to encapsulate PCM can be explored in future. Molecular dynamics study and numerical study of heat transfer behaviour of such novel composites for heat storage can also provide fundamental and key information to accelerate research in this area.

CRediT authorship contribution statement

Dudul Das: Conceptualization, Funding acquisition, Investigation, Methodology, Writing – original draft, Data curation, Formal analysis, Visualization. **Ondrej Masek:** Resources, Writing – review & editing. **Manosh C. Paul:** Conceptualization, Funding acquisition, Project administration, Resources, Supervision, Writing – review & editing.

Declaration of competing interest

The authors declare the following financial interests/personal

relationships which may be considered as potential competing interests: Dudul Das reports financial support was provided by UK Research and Innovation. Manosh Paul reports financial support was provided by UK Research and Innovation. If there are other authors, they declare that they have no known competing financial interests or personal relationships that could have appeared to influence the work reported in this paper.

Data availability

The data that support the findings of this study will be available from the corresponding author upon reasonable request.

Acknowledgement

The research is funded through UK's Engineering and Physical Sciences Research Council (EPSRC) (EP/X027783/1), European Union Marie Skłodowska-Curie Actions (EU MSCA) Fellowship (101063361). The authors would also like to acknowledge Supergen Bioenergy Impact Hub, UKRI/EPSRC/BBSRC (EP/Y016300/1).

References

[1] Renewable Energy Agency I, Innovation Outlook Thermal Energy Storage About IRENA, 2020.
[2] Global Markets Insights. Phase Change Materials Market Size, 2020.
[3] Y. Huang, A. Stonehouse, C. Abeykoon, Encapsulation methods for phase change materials – a critical review, Int J Heat Mass Transf (2023) 200, https://doi.org/10.1016/j.ijheatmasstransfer.2022.123458.
[4] A.K. Mishra, B.B. Lahiri, J. Philip, Carbon black nano particle loaded lauric acid-based form-stable phase change material with enhanced thermal conductivity and photo-thermal conversion for thermal energy storage, Energy (2020) 191, https://doi.org/10.1016/j.energy.2019.116572.
[5] A. Alagumalai, O. Mahian, Specialty grand challenge in thermal science and energy systems, Front. Therm. Eng. (2022) 2, https://doi.org/10.3389/fther.2022.954511.
[6] G. Hekimoğlu, M. Nas, M. Ouikhalfan, A. Sarı, V.V. Tyagi, R.K. Sharma, et al., Silica fume/capric acid-stearic acid PCM included-cementitious composite for thermal controlling of buildings: thermal energy storage and mechanical properties, Energy (2021) 219, https://doi.org/10.1016/j.energy.2020.119588.
[7] Y. Chen, Z. Cui, H. Ding, Y. Wan, Z. Tang, J. Gao, Cost-effective biochar produced from agricultural residues and its application for preparation of high performance form-stable phase change material via simple method, Int. J. Mol. Sci. (2018) 19, https://doi.org/10.3390/ijms19103055.
[8] R.K. Banik, P. Kalita, Enrichment of fuel properties of biomass using non-oxidative torrefaction for gasification, Journal of Renewable and Sustainable Energy 15 (2023) 063102, https://doi.org/10.1063/5.0168553.
[9] K. Wilson, How biochar works in soil, The Biochar Journal (2014) 25–33, biochar-journal.org/en/ct/32,.
[10] U. Bordoloi, D. Das, D. Kashyap, D. Patwa, P. Bora, H.H. Muigai, et al., Synthesis and comparative analysis of biochar based form-stable phase change materials for thermal management of buildings, J Energy Storage (2022) 55, https://doi.org/10.1016/j.est.2022.105801.
[11] D. Das, U. Bordoloi, A.D. Kamble, H.H. Muigai, R.K. Pai, P. Kalita, Performance investigation of a rectangular spiral flow PV/T collector with a novel form-stable composite material, Appl. Therm. Eng. 182 (2021) 116035, https://doi.org/10.1016/j.applthermaleng.2020.116035.
[12] D. Das, U. Bordoloi, H.H. Muigai, P. Kalita, A novel form stable PCM based bio composite material for solar thermal energy storage applications, J Energy Storage 30 (2020) 101403, https://doi.org/10.1016/j.est.2020.101403.
[13] G. Hekimoğlu, A. Sarı, T. Kar, S. Keleş, K. Kaygusuz, V.V. Tyagi, et al., Walnut shell derived bio-carbon/methyl palmitate as novel composite phase change material with enhanced thermal energy storage properties, J Energy Storage (2021) 35, https://doi.org/10.1016/j.est.2021.102288.
[14] G. Hekimoğlu, A. Sarı, S. Arunachalam, H. Arslanoğlu, O. Gencel, Porous biochar/heptadecane composite phase change material with leak-proof, high thermal energy storage capacity and enhanced thermal conductivity, Powder Technol. 394 (2021) 1017–1025, https://doi.org/10.1016/j.powtec.2021.09.030.
[15] L. Cheng, J. Feng, Form-stable phase change materials based on delignified wood flour for thermal management of buildings, Compos. Part A Appl. Sci. Manuf. (2020) 129, https://doi.org/10.1016/j.compositesa.2019.105690.
[16] X. Gu, P. Liu, C. Liu, L. Peng, H. He, A novel form-stable phase change material of palmitic acid-carbonized pepper straw for thermal energy storage, Mater. Lett. 248 (2019) 12–15, https://doi.org/10.1016/j.matlet.2019.03.130.
[17] C. Yin, L. Weng, Z.X. Fei, L.Y. Shi, K.K. Yang, Form-stable phase change composites based on porous carbon derived from polyacrylonitrile hydrogel, Chem. Eng. J. (2022) 431, https://doi.org/10.1016/j.cej.2021.134206.
[18] P.P. Zhao, C. Deng, Z.Y. Zhao, P. Lu, S. He, Y.Z. Wang, Hypophosphite tailored graphitized hierarchical porous biochar toward highly efficient solar thermal energy harvesting and stable storage/release, Chem. Eng. J. (2021) 420, https://doi.org/10.1016/j.cej.2021.129942.
[19] L. Lv, J. Wang, M. Ji, Y. Zhang, S. Huang, K. Cen, et al., Effect of structural characteristics and surface functional groups of biochar on thermal properties of different organic phase change materials: dominant encapsulation mechanisms, Renew. Energy 195 (2022) 1238–1252, https://doi.org/10.1016/j.renene.2022.06.117.
[20] P. Maziarka, C. Wurzer, P.J. Arauzo, A. Dieguez-Alonso, O. Mašek, F. Ronsse, Do you BET on routine? The reliability of N2 physisorption for the quantitative assessment of biochar's surface area, Chem. Eng. J. (2021) 418, https://doi.org/10.1016/j.cej.2021.129234.
[21] O. Mašek, W. Buss, A. Roy-Poirier, W. Lowe, C. Peters, P. Brownsort, et al., Consistency of biochar properties over time and production scales: a characterisation of standard materials, J. Anal. Appl. Pyrolysis 132 (2018) 200–210, https://doi.org/10.1016/j.jaap.2018.02.020.
[22] Sofies. The Biochar Network-Demonstrating a Scalable GGR Solution Final Report. n.d.
[23] V. Shanmugam, S.N. Sreenivasan, R.A. Mensah, M. Försth, G. Sas, M.S. Hedenqvist, et al., A review on combustion and mechanical behaviour of pyrolysis biochar, Mater Today Commun (2022) 31, https://doi.org/10.1016/j.mtcomm.2022.103629.
[24] M.U. Babler, A. Phounglamcheik, M. Amovic, R. Ljunggren, K. Engvall, Modeling and pilot plant runs of slow biomass pyrolysis in a rotary kiln, Appl. Energy 207 (2017) 123–133, https://doi.org/10.1016/j.apenergy.2017.06.034.
[25] X.Y.D. Soo, Z.M. Png, M.H. Chua, J.C.C. Yeo, P.J. Ong, S. Wang, et al., A highly flexible form-stable silicone-octadecane PCM composite for heat harvesting, Mater Today Adv (2022) 14, https://doi.org/10.1016/j.mtadv.2022.100227.
[26] R. Yang, X. Guo, H. Wu, W. Kang, K. Song, Y. Li, et al., Anisotropic hemp-stem-derived biochar supported phase change materials with efficient solar-thermal energy conversion and storage, Biochar 4 (2022) 38, https://doi.org/10.1007/s42773-022-00162-1.
[27] J. Rouquerol, F. Rouquerol, P. Llewellyn, G. Maurin, K. Sing, Adsorption by Powders and Porous Solids: Principles, Methodology and Applications, Academic Press, 2013.
[28] L. Wang, M.N.P. Olsen, C. Moni, A. Dieguez-Alonso, J.M. de la Rosa, M. Stenrød, et al., Comparison of properties of biochar produced from different types of lignocellulosic biomass by slow pyrolysis at 600 °C, Applications in Energy and Combustion Science 12 (2022) 100090, https://doi.org/10.1016/j.jaecs.2022.100090.
[29] D.G. Atinafu, S. Jin Chang, K.H. Kim, S. Kim, Tuning surface functionality of standard biochars and the resulting uplift capacity of loading/energy storage for organic phase change materials, Chem. Eng. J. (2020) 394, https://doi.org/10.1016/j.cej.2020.125049.
[30] B.K. Ramaraj, R.K. Kottala, Preparation and characterisation of binary eutectic phase change material/activated porous bio char/multi walled carbon nano tubes as composite phase change material, Fullerenes Nanotubes and Carbon Nanostructures 31 (2023) 75–89, https://doi.org/10.1080/1536383X.2022.2123800.
[31] Y. Qian, N. Han, Z. Zhang, R. Cao, L. Tan, W. Li, et al., Enhanced thermal-to-flexible phase change materials based on cellulose/modified graphene composites for thermal management of solar energy, ACS Appl. Mater. Interfaces 11 (2019) 45832–45843, https://doi.org/10.1021/acsami.9b18543.
[32] Z. An, H. Chen, X. Du, T. Shi, D. Zhang, Preparation and performance analysis of form-stable composite phase change materials with different EG particle sizes and mass fractions for thermal energy storage, ACS Omega 7 (2022) 34436–34448, https://doi.org/10.1021/acsomega.2c04101.
[33] P. Lv, C. Liu, Z. Rao, Experiment study on the thermal properties of paraffin/kaolin thermal energy storage form-stable phase change materials, Appl. Energy 182 (2016) 475–487, https://doi.org/10.1016/j.apenergy.2016.08.147.
[34] D.G. Atinafu, S. Wi, B.Y. Yun, S. Kim, Engineering biochar with multiwalled carbon nanotube for efficient phase change material encapsulation and thermal energy storage, Energy (2021) 216, https://doi.org/10.1016/j.energy.2020.119294.
[35] Y.C. Wan, Y. Chen, Z.X. Cui, H. Ding, S.F. Gao, Z. Han, et al., A promising form-stable phase change material prepared using cost effective pinecone biochar as the matrix of palmitic acid for thermal energy storage, Sci. Rep. (2019) 9, https://doi.org/10.1038/s41598-019-47877-z.
[36] S. Mandal, S. Ishak, D.-E. Lee, T. Park, Shape-stabilized orange peel/myristic acid phase change materials for efficient thermal energy storage application, Energy Rep. 8 (2022) 9618–9628, https://doi.org/10.1016/j.egyr.2022.07.143.
[37] J. Jeon, J.H. Park, S. Wi, S. Yang, Y.S. Ok, S. Kim, Characterization of biocomposite using coconut oil impregnated biochar as latent heat storage insulation, Chemosphere 236 (2019) 124269, https://doi.org/10.1016/j.chemosphere.2019.06.239.
[38] Q. He, H. Fei, J. Zhou, X. Liang, Y. Pan, Utilization of carbonized water hyacinth for effective encapsulation and thermal conductivity enhancement of phase change energy storage materials, Construct. Build Mater. 372 (2023) 130841, https://doi.org/10.1016/j.conbuildmat.2023.130841.
[39] A. Anand, A. Shukla, A. Kumar, D. Buddhi, A. Sharma, Cycle test stability and corrosion evaluation of phase change materials used in thermal energy storage systems, J Energy Storage (2021) 39, https://doi.org/10.1016/j.est.2021.102664.